Reprint

Contributions to Atmospheric Physics

Beiträge zur Physik der Atmosphäre

A publication of the
Deutsche Meteorologische Gesellschaft

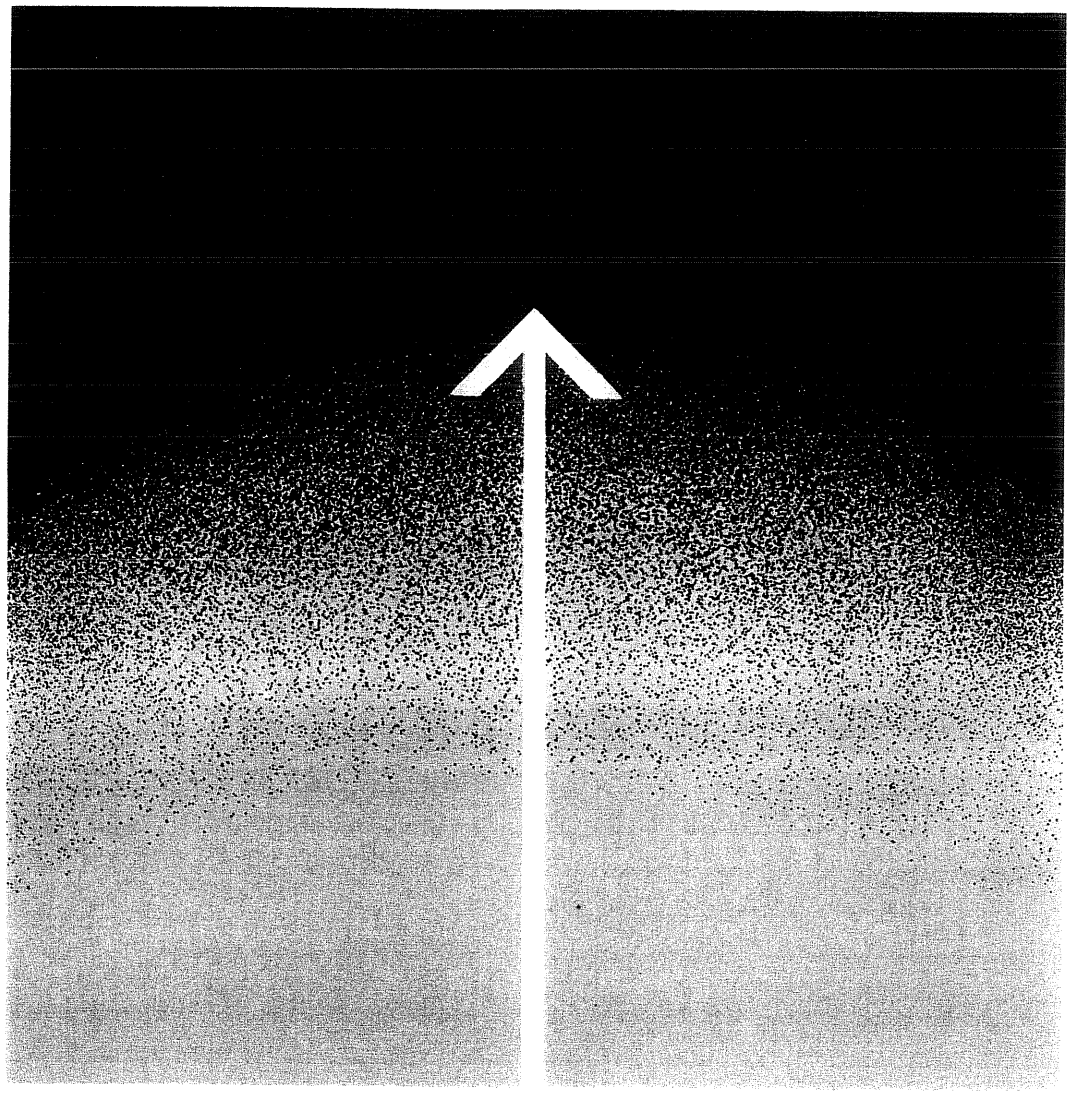

vieweg

Contr. Atmos. Phys., August 1999, p. 205–218
0005-8173/99/03 0205-14 $ 3.00/0

Introducing the Effective Radius into a Fast Radiation Scheme of a Mesoscale Model

KLAUS WYSER[1,4], LAURA RONTU[2], HANNU SAVIJÄRVI[3]

[1] Department of Meteorology, Stockholm University, 10691 Stockholm, Sweden
[2] Finnish Meteorological Institute, P.O. Box 503, 00101 Helsinki, Finland
[3] Department of Meteorology, P.O. Box 4, 00014 University of Helsinki, Finland
[4] present affilation: Institute for Computational Earth System Science, UC Santa Barbara, Santa Barbara, CA 93106-3060, USA

(Manuscript received March 05, 1998; accepted September 11, 1998)

Abstract

The effective radius r_e describing the size of cloud droplets and ice crystals is derived from the cloud condensate content and temperature calculated within the HIRLAM short-range numerical weather prediction model. Introducing r_e into the radiation scheme of the model allows the scheme to handle clouds with different sizes of cloud droplets and ice crystals in a realistic way. The modification to the radiation scheme retains the fast performance of the scheme. Using the droplet size information mainly affects the short-wave radiation of thin clouds. On the average, the ice clouds become slightly more and the water clouds slightly less transparent than in the original radiation scheme. In general, the effect of the new parametrization on the synoptic-scale forecast is small, but local changes in the model's two-metre temperature can be significant.

1 Introduction

The radiative properties of clouds depend strongly on the size of the cloud particles (Slingo, 1989; Slingo, 1990; Kiehl, 1994; Chen and Ramaswamy, 1996). Hu and Stamnes (1993) demonstrated that the effective radius (r_e) is a good measure of the average particle size for radiation purposes, at least for spherical water droplets. Numerous parametrizations for the optical properties of clouds in terms of r_e have been suggested, both for water (Slingo, 1989; Hu and Stamnes, 1993; Savijärvi et al., 1997) and ice clouds (Ebert and Curry, 1992; Fu, 1996).

The problem remains as to what value to assign to r_e. Satellite retrievals and other observations reveal that the droplet size, and thus r_e, varies with location, the main variability being due to differences between continental and maritime air masses (Han et al., 1994) The differences between r_e over land and sea are relevant for the Earth's climate, as has been found in a sensitivity experiment with the NCAR GCM (Kiehl, 1994). The findings have been confirmed in a study with the ARPEGE model (Dandin et al., 1997).

It is possible to prescribe r_e and treat it as a tuneable parameter in large-scale models, for example those used in the studies by Kiehl (1994) and Chen and Ramaswamy (1996). However, a more physical solution is preferable that accounts for the variability of r_e with ambient conditions. Several attempts have been explored how to relate r_e and the cloud condensate content (*CCC*) in water clouds (Bower et al., 1994; Martin et al., 1994; Pontikis, 1996; Wyser, 1998b). In all these approaches the amount of cloud condensate is divided by the number of droplets to find the mean volume of a droplet which is assumed to be proportional to r_e. Another method is to develop a parameterization from observations of the effective radius and other atmospheric variables (Gultepe and Isaac, 1996; Gultepe et al., 1996). However, parameterizations based on statistical fits are difficult to generalise as they, in principle, are valid only for the same conditions under which the observations have been made.

Finding the effective radius is more difficult for ice clouds than for liquid water clouds. The main problem is the nonspherical shape of the ice crystal which makes the definition of an effective radius ambiguous (Wyser, 1998a). A number of observations have revealed that the mean size of ice crystals decreases with temperature in a statistical way (Heymsfield and Platt, 1984). Subsequently, the effective radius for ice crystals could be expressed as a function of the temperature (Ou and Liou, 1995). Other parameterizations of r_e for ice clouds have been suggested that also take into account the ice water content (Westphal et al., 1996; Wyser, 1998a). In this study, however, the simpler parameterization that only depends on the temperature is used to keep the computational effort low. Some tests with a more sophisticated parameterization did not reveal substantial differences in the radiative fluxes.

How important is the effective radius in numerical weather prediction models? This question has not been answered comprehensively yet. A previous case study with the HIRLAM (High Resolution Limited Area Model) forecast model was done to explore how a decrease in r_e from 10 μm to 5 μm affects a 15 hour forecast. The smaller droplets increase the reflectivity of the clouds, more sunlight is reflected back to space and less reaches the surface. As a consequence, the surface temperature becomes lower for small-drop clouds, the decrease exceeding 0.5 K over large areas. The effect on long-wave radiation is much smaller, since thick model clouds tend to be black bodies irrespective of the droplet size, except possibly cirrus clouds.

The radiative transfer in HIRLAM is calculated with a very fast scheme (Sass et al., 1994). This is achieved by highly parametrizing the interaction between the atmosphere and the radiation. The short-wave absorptivity and transmissivity of clouds are parametrized in terms of the cloud condensate amount, with a fixed r_e of about 10 μm. The objective of the present study is to modify the parametrization to allow for variations in the effective radius. Another refinement is achieved by treating the radiative properties of water and ice clouds separately. All changes are made in such a way that the fast performance of the scheme is not affected.

The present study is organised as follows: the retrieval of r_e for water clouds and for ice clouds is described in Section 2. Section 3 gives a brief overview of the present HIRLAM cloud and radiation schemes. The changes needed to include r_e as a further parameter to the radiation scheme are discussed in Section 4. A number of experiments with the modified radiation scheme are presented in Section 5. Conclusions and an outlook in Section 6 complete this study.

2 A parametrization for r_e

2.1 Water clouds

Martin et al. (1994) found empirically a linear relationship between the cubes of the mean volume radius r_v and the effective radius,

$$r_{e,water}^3 = k r_v^3. \tag{2.1}$$

The parameter k is found to be different for marine and continental clouds – values are given in Table 1. Assuming spherical droplets, the cloud condensate content (CCC = liquid + ice water content, in kg m^{-3}) is connected to r_v by

$$CCC = \frac{4\pi}{3} \rho_\ell N r_v^3 \tag{2.2}$$

where $\rho_\ell = 1000\,\mathrm{kg\,m^{-3}}$ is the density of liquid water and N the number concentration of the cloud droplets. Suggested values of N for marine and continental clouds are also listed in Table 1. Combining (2.1) and (2.2) yields

$$r_{e,water} = \left(\frac{3CCC}{4\pi\rho_\ell k N} \right)^{1/3} \tag{2.3}$$

which allows one to calculate $r_{e,water}$ for spherical droplets from the cloud condensate content. Figure 1 shows the relation between CCC and $r_{e,water}$ together with some values from different cloud droplet size distributions. Note that (2.3) might underestimate $r_{e,water}$ for low cloud condensate amounts. Theory predicts that small droplets grow relatively faster than large droplets by diffusion. Thus, all small droplets will rapidly grow to a certain size as soon as they are activated. A minimum $r_{e,min} = 4\,\mu\mathrm{m}$ is introduced to account for the resulting low abundance of small droplets.

The different values for k and N are due to the higher concentrations of cloud concentration nuclei (CCN) over land surfaces. The marine values are representative of clean background air, as may be found over

Table 1: Parameters for the calculation of $r_{e,water}$ as suggested by Wyser (1998b).

	k	N [m^{-3}]
marine	0.81	1×10^8
continental	0.69	4×10^8

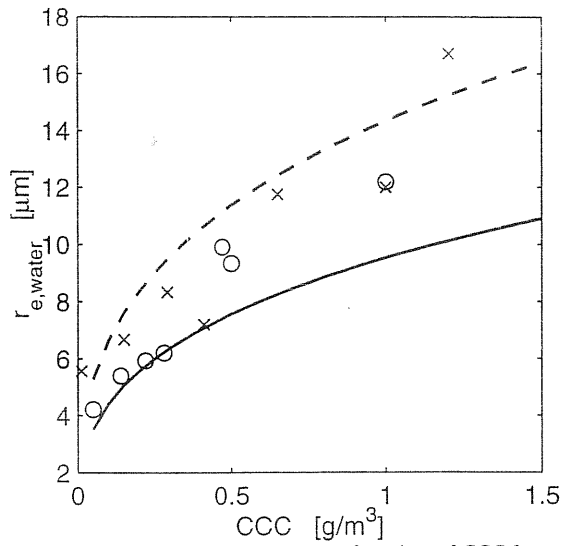

Figure 1: Effective radius $r_{e,water}$ as a function of *CCC* for continental (solid) and marine (dashed) clouds. Also shown are values cited by Slingo and Schrecker (1982) and Chylek et al. (1992) as circles and crosses, respectively.

oceans. Upper tropospheric air is also considered to be clean and the marine values for k and N are applied there, too. The variability of *CCN* in space is accounted for by weighting r_e accordingly,

$$r_{e,water} = f r_{e,cont} + (1-f) r_{e,mar}, \qquad (2.4)$$

where $r_{e,cont}$ and $r_{e,mar}$ are the effective radii calculated with the parameter values for continental and marine clouds, respectively. The weight f depends on height and location, a coarse approximation is

$$f = \begin{cases} f_{land}(\eta - \eta_0)/(1-\eta_0) & \eta > \eta_0 \\ 0 & \eta \le \eta_0 \end{cases} \qquad (2.5)$$

where f_{land} is the fraction of land at a gridpoint and η is the vertical hybrid coordinate decreasing from $\eta = 1$ at the surface to $\eta = 0$ at the top of the model atmosphere. The threshold value η_0 describes how far the higher concentration of aerosols over land affects the droplet concentration. For the present study, η_0 is set to 0.7.

2.2 Ice Clouds

Ice clouds are difficult to observe, and data about the size and shape of ice particles are sparse. Another problem is how to define an effective radius for non-spherical ice crystals (Wyser, 1998a). Ou and Liou (1995) suggest to link the mean effective width D_e to the cloud temperature based on the observations by Heymsfield and Platt (1984). The resulting parameterization becomes

$$D_e = 326.3 + 12.42 T_c + 0.197 T_c^2 + 0.0012 T_c^3 \qquad (2.6)$$

where T_c is in °C and D_e in μm (Ou and Liou, 1995). The effective radius is obtained by assuming $r_{e,ice} = D_e/2$. Note that (2.6) has been obtained as a cubic polynomial fit to observed data below −20°C, and extrapolating (2.6) to higher temperatures might lead to unreasonably high values for $r_{e,ice}$. Thus, the minimum of −20°C and the ambient temperature is taken in (2.6), resulting in an upper limit for $r_{e,ice}$ of about 75 μm.

3 Cloud and radiation parametrizations in HIRLAM

In the HIRLAM model cloud-radiation interactions are handled by the condensation and radiation routines. These are a part of the physical parametrizations of the model, including also parametrizations of turbulent and soil-surface processes.

3.1 Cloud scheme

The HIRLAM cloud scheme is based on Sundqvist et al. (1989) and Sundqvist (1993), and is documented in Källen (1996). One part of the scheme parametrizes the release of latent heat (production of condensate) and connected subgrid-scale circulation (fractional cloud cover). The other part deals with microphysical processes, i.e. the release of precipitation, and the evaporation and melting of hydrometeors. Values of cloud condensate content, fractional cloud cover and probability of ice given by the cloud scheme are used as input for the radiation scheme in HIRLAM.

The cloud condensate content is a prognostic variable in the model. The fractional cloud cover is derived from the relative humidity values independently of the cloud condensate content. Different schemes for stratiform and convective cloud cover are used. The ice water content is approximated by multiplying the cloud condensate content by the probability of ice. The ice probability f_{ice} is given as a function of temperature (Sundqvist (1993), based on the work of Matjevev (1994)).

3.2 Radiation scheme

The HIRLAM radiation scheme is documented in Sass et al. (1994). It is based on Savijärvi (1990); only a brief overview is given here. The scheme

was designed to be fast, so only one vertical loop is allowed in both the solar (short-wave, SW) and the thermal (long-wave, LW) part. The SW clear-air global flux is obtained by reducing the top-of-the-atmosphere (TOA) horizontal flux by broadband average ozone absorption (350 DU), water vapour absorption (depending on the scaled precipitable water content u), and Rayleigh scattering in the column. Average aerosol, CO_2, and O_2 effects are also included. In cloudy air the SW flux is reduced by the total cloud transmissivity $\hat{T}$, also taking into account multiple reflections between cloudbase and the surface. In a partly cloudy column the clear-sky and cloudy sky results are linearly combined.

The cloud SW transmissivity and absorptivity functions are fits to detailed multiple scattering scheme calculations (Stephens, 1978; Liou and Wittmann, 1979; Slingo, 1989; Ramaswamy and Freidenreich, 1992) for stratus-type clouds with an effective drop radius of about 10 μm. The functions depend on the solar zenith angle θ and the modified cloud condensate amount $\hat{M}$ (in g m^{-2}), which is the vertical integral above the level under consideration of CCC multiplied by the relation of the cloud cover C to the maximum cloud cover of the whole column C_{max},

$$\hat{M}(z) = C_{max}^{-1} \int_z^{\mathrm{TOA}} CCC(z')C(z')\,dz'. \tag{3.1}$$

The absorptivity is

$$\hat{A} = b_{10}(b_{11} + \cos\theta)\log(1 + b_{12}\hat{M}) \tag{3.2}$$

with the parameters $b_{10} = 0.013$, $b_{11} = 1$, and $b_{12} = 0.1\,\mathrm{m^2\,g^{-1}}$. The transmissivity is given by

$$\hat{T} = \hat{T}_1 / (\hat{T}_1 + \hat{M}) \tag{3.3}$$

where

$$\hat{T}_1 = b_{13}(b_{14} + \cos\theta) \tag{3.4}$$

with the parameters $b_{13} = 40\,\mathrm{gm^{-2}}$ and $b_{14} = 0.5$.

Clear-air solar heating due to water vapour absorption, $a(u)$, is obtained by vertical flux convergence, fitting $\partial a/\partial u$ from the line-by-line $a(u)$ curves of Chou (1986). In and below clouds the clear-air values are reduced by the cloud transmittance $\hat{T}$. In clouds there is also extra heating due to cloud drop absorption, represented by the flux convergence of the absorptivity, $\partial\hat{A}/\partial p$.

Ice clouds are not treated separately in the SW scheme. All clouds are considered to consist of liquid water droplets.

The LW part uses a broadband emissivity scheme in a local isothermal approximation. The water vapour line emissivity is a cubic function of $\log u$; continuum, CO_2, and O_3 effects are added as extra terms. There can be clouds both above and below the layer in question. Cloud effective emissivity ε is

$$\varepsilon = C(1 - \exp(-k_a m)), \tag{3.5}$$

where C is the fractional cloud cover, $m = CCC\Delta z$ is the cloud condensate amount (in gm^{-2}) of the layer with a thickness Δz, and the cloud mass absorption coefficient k_a decreases linearly with the vertical hybrid η coordinate, so as to give smaller values for ice clouds as is observed. Near the surface k_a is 0.20 m^2 g^{-1}, and near the tropopause 0.05 m^2 g^{-1}.

4 Modifications of the radiation scheme

4.1 Short-wave radiation

In order to retain the fast performance of the HIRLAM radiation scheme, only small modifications are looked for that do not change the basic features of the scheme. It is suggested that the functional form of the SW cloud absorption and transmission be left unchanged, except for the parameters b_{10} and b_{13}, (c.f. Eqs. 3.2–3.4), that now depend on $r_{e,\mathrm{SW}}$,

$$\begin{aligned} b_{10} &= b_{10a} r_{e,\mathrm{SW}} + b_{10b}, \\ b_{13} &= b_{13a} r_{e,\mathrm{SW}} + b_{13b}, \end{aligned} \tag{4.1}$$

where $r_{e,\mathrm{SW}}$ is the effective radius for short-wave calculations (see Section 4.1.3). Values for all the b-parameters are found by adjusting the HIRLAM radiation scheme to a more sophisticated radiative transfer model.

4.1.1 Water clouds

Cloud absorption and transmission is calculated for various water paths, effective radii, and solar zenith angles with a two-stream 5-band radiative transfer model. The model is a modification of the 4-band model briefly described in Savijärvi et al. (1997) but with the cloud optics derived from Hu and Stamnes (1993). The HIRLAM parametrizations (3.2) and (3.3) for absorption and transmission with modifications (4.1) are then fitted to the results from the more detailed radiative transfer model by minimising the sum of the least square differences. Figure 2 shows an example of the transmission calculated with the detailed radiation model compared to the HIRLAM parameterization. The new values for the SW coefficients are listed in Table 2. Note that that the values of all b-parameters change, not only b_{10} and b_{13}.

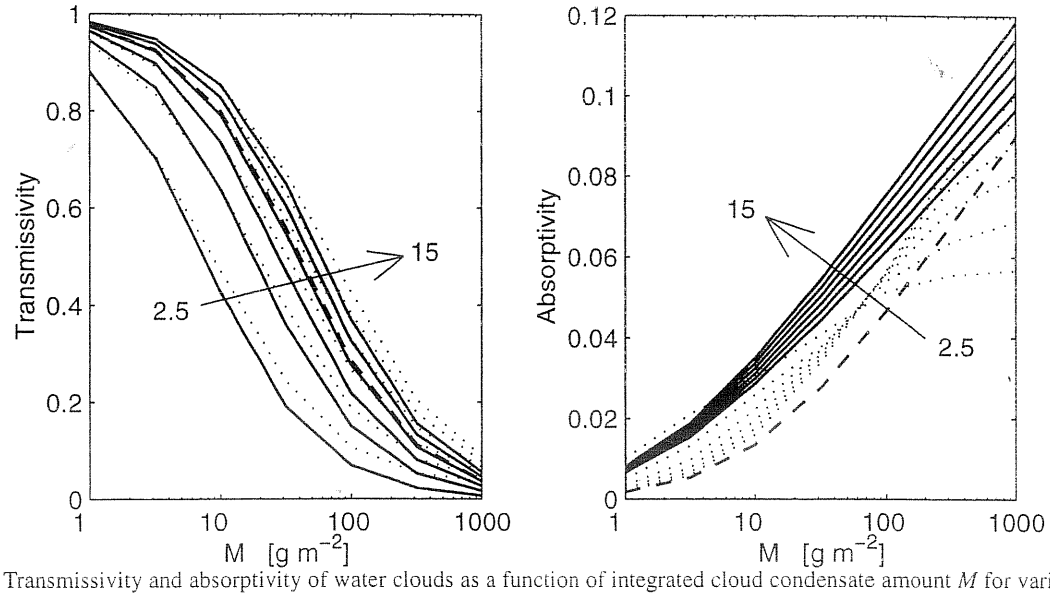

Figure 2: Transmissivity and absorptivity of water clouds as a function of integrated cloud condensate amount M for various $r_{e,water}$ at a zenith angle of 60°. Shown are results from the 5-band radiative transfer model (dotted), the old (dashed) and the new (solid) HIRLAM parametrizations. The arrow indicates the direction of increasing $r_{e,water}$, with the lowest and highest values of 2.5 and 15 μm, respectively. The increment between the curves is 2.5 μm.

Table 2: Parameters for the SW scheme to be used in (4.1) valid for $r_{e,water}$ given in μm and $\hat{M}$ in g m^{-2}.

Absorption		Transmission	
b_{10a}	1.55×10^{-4}	b_{13a}	7.00
b_{10b}	8.18×10^{-3}	b_{13b}	-4.75
b_{11}	1.29	b_{14}	8.30×10^{-2}
b_{12}	0.545		

Table 3: Parameters for the conversion between $r_{e,ice}$ and r_{eq}, valid for radii given in μm.

a_1	0.522
a_2	-4.551
a_3	4.115

4.1.2 Ice clouds

Ice clouds are included in the SW parametrization through an equivalent radius, r_{eq}. This radius is chosen in such a way that an ice cloud with particles of size $r_{e,ice}$ has the same optical properties as a water cloud with $r_{e,water} = r_{eq}$. Assuming

$$r_{eq} = a_1 r_{e,ice} + a_2 \cos\theta + a_3, \tag{4.2}$$

for the relation between $r_{e,ice}$ and r_{eq}, we look for values of the coefficients a_i in the following way: the transmissivity $\hat{T}$ for a number of ice clouds is calculated with the 5-band radiative transfer model with ice optics from Ebert and Curry (1992). The a-parameters are then found by matching the HIRLAM transmissivity as defined by (3.3) and (3.4) with the new values for b and $r_e = r_{eq}$ to the result from the radiative transfer model. The values for the a-parameters are listed in Table 3.

4.1.3 Effective radius for SW calculations

The effective radius for the SW calculations, $r_{e,\mathrm{SW}}$, is determined from $r_{e,water}$ and r_{eq}. Special treatment is necessary, since $r_{e,\mathrm{SW}}$ should be representative not only of the level under consideration but also of all the cloud water and cloud ice above, as multiple scattering between cloud layers is not taken into account explicitly. Therefore, an effective radius weighted by the cloud condensate amount, cloud cover and thickness of each layer is calculated:

$$r_{e,\mathrm{SW}}(j) = \frac{\sum_{i=1}^{j} [r_{e,water}(i)(1 - f_{ice}(i)) + r_{eq}(i) f_{ice}(i)]\, C(i) CCC(i) \Delta z(i)}{\sum_{i=1}^{j} CCC(i) C(i) \Delta z(i)}, \tag{4.3}$$

where $C(i)$ is the cloud cover and $\Delta z(i)$ the thickness of the layer i. Note that the summation extends from TOA ($i = 1$) to the level under consideration.

4.2 Long-wave radiation

The cloud mass absorption coefficient k_a in the reference HIRLAM is a function of normalised pressure only. Here, it is modified to depend on the effective radius explicitly,

$$k_{a,x} = c_1 + c_2 \exp(-c_3 r_{e,x}) \quad (4.4)$$

where the index x stands for either water or ice. Expression (4.4) is taken from ECHAM 4 (Roeckner et al., 1996). The values for the c-parameters are given in Table 4 and are valid for $r_{e,x}$ given in μm and $k_{a,x}$ in $m^2\ g^{-1}$. The total mass absorption coefficient is composed of water and ice contributions. The effective emissivity ε of a cloudy layer now becomes

$$\varepsilon = C\{1 - \exp[-(k_{a,water} m_w + k_{a,ice} m_i)]\}, \quad (4.5)$$

where $m_w = (1 - f_{ice})CCC\Delta z$ and $m_i = f_{ice} CCC\Delta z$ are the cloud water and cloud ice amounts (in gm^{-2}) of the layer.

Table 4: Parameters for the cloud LW mass absorption coefficient from ECHAM 4 (Roeckner et al., 1996).

	Water	Ice
c_1	0.0255	0.0202
c_2	0.2855	0.2059
c_3	0.0890	0.0676

5 Model experiments

The reference HIRLAM radiation scheme (Sass et al., 1994) was validated using data from the Intercomparison of Radiation Codes used in Climate Models (ICRCCM, Ellingson et al., 1991) and measurements of the Joint Air-Sea Interaction experiment (JASIS, Slingo et al. 1982). Part of the same data is used here to test the effect of introducing drop size information into the scheme. The sensitivity of the radiation scheme to variations in the cloud condensate vertical distribution is illustrated after the comparisons. In addition, surface radiation flux measurements from a Southern Finland observatory (Jokioinen) are compared with one-dimensional HIRLAM calculations using collocated aerological sounding data as input. An example of the influence of radiation parametrizations in a full HIRLAM forecast is shown.

In the following, the reference HIRLAM scheme will be called 'H2 old' and the scheme with the variable effective radius, described above, 'H2 new'.

5.1 The ICRCCM comparisons

Four different single-layer clouds were considered in the ICRCCM comparisons: high and low (heights 1-2 km and 9-10 km), and thin and thick (cloud water path 10 and 200 $g\ m^{-2}$) clouds. All clouds were assumed to be water clouds irrespective of their height. Two cloud types with small (CS, $r_{e,water}$ = 5.25 μm) and large (CL, $r_{e,water}$ = 31 μm) drops were defined. The mid-latitude summer atmosphere with a solar zenith angle of 30°, surface albedo 0.2 and surface emissivity 1 is used here. The full ICRCCM data sets can be found in Ellingson and Fouquart (1991). All gases and aerosols were included in the HIRLAM calculations. The profiles were interpolated to the 31 hybrid levels of HIRLAM. The low clouds were assumed to lie between the levels 769 and 915 hPa and the high clouds between the levels 173 and 237 hPa. The results are compared against the ICRCCM average values, pending better references.

The downward surface fluxes are shown in Table 5. The effect of the new parametrization is best seen in the short-wave fluxes, where the difference between the CS and CL clouds is significant and is well reproduced by the 'H2 new' scheme. The long-wave fluxes given by 'H2 new' differ from those of 'H2 old' only in the case of thin clouds, where the difference between large-drop and small-drop clouds given by 'H2 new' is somewhat larger than in the average ICRCCM results.

Table 5: Downward radiative fluxes at the surface for the ICRCCM clouds.

SW down ($W\ m^{-2}$)	low thin	low thick	high thin	high thick
ICRCCM CS	782±31	-	779±31	-
ICRCCM CL	921±18	537±48	920±18	536±54
H2 old	814	251	853	241
H2 new CS	767	153	760	149
H2 new CL	892	525	930	529
LW down ($W\ m^{-2}$)				
ICRCCM CS	399±8	-	360±7	-
ICRCCM CL	389±11	413±3	358±7	363±7
H2 old	409	416	356	371
H2 new CS	408	416	368	371
H2 new CL	378	416	358	371

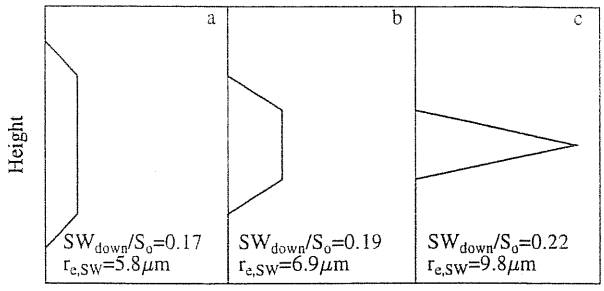

Figure 3: Schematic vertical distributions of cloud condensate content. The diagnosed effective radius $r_{e,SW}$ at the lowest cloud level and the ratio of downward short-wave radiation flux at the surface to the top-of-atmosphere flux SW_{down}/S_o are shown in each panel.

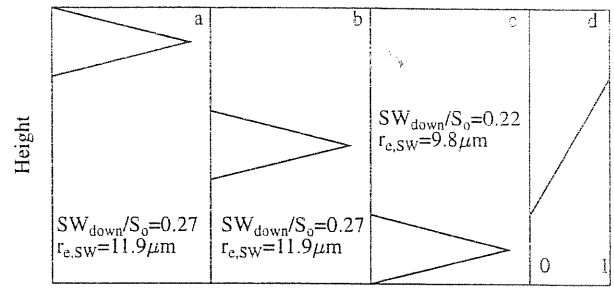

Figure 4: Schematic vertical distributions of cloud condensate, the diagnosed effective radius $r_{e,SW}$ at the lowest cloud level and the corresponding ratio of downward short-wave radiation flux at the surface to the top-of-atmosphere flux SW_{down}/S_o (a-c). The vertical profile of ice probability valid in all cases is shown in (d).

5.2 A sensitivity example

The ICRCCM mid-latitude summer atmosphere with a solar zenith angle of 30° and a total cloud condensate content of 200 g m^{-2} was used in the sensitivity study. In Figure 3, three different schematic vertical distributions of cloud condensate and the corresponding calculated with the 'H2 new' scheme ratio of downward short-wave radiation flux at the surface to the top-of-atmosphere flux SW_{down}/S_o are shown.

In the 'H2 old' scheme, the surface fluxes depend only on the total cloud condensate content and the relation SW_{down}/S_o is 0.20 for all cases in Figures 3 and 4. Introducing the effective droplet radius derived from the cloud condensate content makes the 'H2 new' scheme sensitive also to the vertical distribution of cloud condensate. Geometrically thick but less dense water cloud (Figure 3a) now contains small droplets and thus reflects more short-wave radiation than the cloud with the same cloud condensate amount concentrated in a thin layer (Figure 3c) and thus consisting of large drops. Because of this physically based behaviour, the new scheme can be more sensitive to the inaccuracies due to the model vertical resolution.

The effect of introducing a parametrization of ice effects on short-wave radiation is illustrated in Figure 4. The downward short-wave flux at the surface is smallest below a low all-water cloud. High ice clouds and the mixed middle clouds with the same cloud condensate content transmit more short-wave radiation to the surface. The radiation scheme thus becomes more sensitive to the vertical location of the cloud layer and also to the form of the temperature-dependent ice probability function in the model.

5.3 The JASIN case

Measurements made during the Joint Air-Sea Interaction Experiment in a stratocumulus-capped boundary layer over the Northern Atlantic, 8 August 1978 (Slingo et al., 1992), were used for a detailed comparison of parametrized and observed cloud and radiation parameters. The vertical profiles of temperature, humidity, cloud water and cloud drop size (optional) were used as input data. The measured short-wave and long-wave radiative fluxes were used in validating the model results.

Solar TOA flux was taken equal to 1327 W m^{-2} and solar zenith angle as 43.7° (Slingo et al., 1994). The surface albedo was 0.05 and surface emissivity 1. Above an altitude of 10 km, sub-arctic summer temperature and humidity profiles were used. The cloud was assumed to cover the whole grid box in the horizontal. The model resolution was 181 levels, 8 of which were inside the cloud layer, located between about 560 and 900 metres. The total cloud water content in the cloud was about 130 gm^{-2} and the measured effective drop radius was 10.3 μm at the cloud top, 7.9 μm in the middle and 6.1 μm at the cloud base (Schmetz, 1987). (As diagnosed by the 'H2 new' scheme the effective radius varied from 11.8 μm at the top to 4.3 μm at the base, another parametrization from Savijärvi (1997) giving 10.9 μm to 5.8 μm.)

The net radiation fluxes above, below and inside the cloud are compared in Table 6. The total short-wave absorption and the system albedo (the ratio of upward flux to downward flux at the cloud top level) are shown in Table 7. Estimates of the reliability of the observed fluxes can be found in Slingo et al. (1982). The inaccuracy in defining cloud boundaries in the

Table 6: Net radiative fluxes at some altitudes in the JASIN case.

SW net (W m^{-2})	Above cloud	In cloud	Below cloud
H2 old	275	205...270	205
H2 new/diagnosed reff	305	230...300	230
H2 new/observed reff	270	200...265	200
Obs*	260±50	210...275±40	200±40
Schmetz*	280	235...255	
LW net (W m^{-2})			
H2 old	−85	−7... − 10	−18
H2 new/diagnosed reff	−85	−8... − 10	−18
H2 new/observed reff	−85	−7... − 10	−18
Obs**	−70±4	−10... − 20±4	−20±4
Schmetz and Raschke**	−90	0	−20

*Values from Schmetz (1997), **values from Figure 13 and Table 3 of Slingo et al. (1982). The observation error is related to individual measurements.

Table 7: Total short-wave absorption and system albedo in the JASIN case.

	Total absorption(W m^{-2})	System albedo
H2 old	57	0.66
H2 new/diagnosed reff	66	0.62
H2 new/observed reff	63	0.66
Obs*	52±20	0.68±0.02
Schmetz et al.*	51	0.69
Slingo and Schrecker*	59	0.68

*Values from a Table inserted in Figure 14 of Slingo et al. (1982), based on Schmetz et al. (1981), Slingo and Schrecker (1982).

model and in the observations may cause some additional differences between the modelled and observed results.

The net radiative fluxes and system albedo given by the 'H2 new' scheme using observed drop sizes as input differ from observed fluxes less than 10 W m^{-2}. The diagnosed effective radius, averaged for short-wave calculations (Eq. 4.3), is slightly overestimated near the cloud base. Thus the net short-wave fluxes are about 20–40 W m^{-2} larger and the system albedo smaller than the observed mean values. All fluxes are, however, correct within the observational accuracy. Results obtained using the effective radius parametrized according to Savijärvi (1997) (not shown) do not differ significantly from these. The 'H2 old' scheme also gives good results, because its parametrizations are based on the type of clouds observed here. The total cloud absorption given by the 'H2 new' scheme is somewhat overestimated, both with the observed and diagnosed effective radii. The resulting inaccuracy in the radiation fluxes is small, because the magnitude of cloud absorption is minor compared with the magnitude of reflection from clouds.

The long wave results given by the different schemes are quite similar, the dense stratocumulus layer being close to a black body. The difference between the observed and calculated LW fluxes might be explained by the presence of a thin cloud layer above the stratus deck (Slingo et al., 1982).

5.4 Surface radiation fluxes at Jokioinen

Many of the aerological sounding stations measure surface radiation fluxes continuously. Simultaneous synoptic observations are also available. The sounding data can be used as input to radiation schemes,

and radiation observations can be used for validation of the results in clear sky cases. In cloudy situations a major problem is the lack of measured data of cloud condensate and cloud cover and their vertical distribution. This data could be estimated from the relative humidities of the soundings, as was done for example by Baer et al. (1996). Another possibility is to use the predicted cloud condensate and cloud cover from a NWP model as input to the radiation calculations. The predicted cloud condensate and cloud cover may not correspond exactly to the true values, so direct comparison between observed and predicted radiation fluxes is not possible. However, differences between radiation parametrizations can be revealed, and observations give some guidance to the validation of the results. The latter approach was chosen in this study.

Data from the aerological observatory of Jokioinen (WMO number = 02963), in South-western Finland, were used. Detailed measurements of radiative fluxes at the surface and routine synoptic and aerological sounding data are available. An eight-day cloudy period from 12 UTC 9 July to 00 UTC 18 July, 1989 was chosen for comparison. During the period heavy convective and stratiform cloudiness was frequent.

A one-dimensional version of HIRLAM without time integration was used. The number of vertical levels in the model was 61. The input to the model consisted of measured ground temperatures and profiles of temperature and relative humidity from the soundings. A mean albedo of 0.18, with a correction depending on the solar height angle, and a surface emissivity of 0.98 were used in the one-dimensional calculations. Cloud liquid water and cloud cover (at the nearest grid point) were provided by three-dimensional HIRLAM 12-hour forecasts based on the ECMWF 00 UTC and 12 UTC analyses.

The radiation observations used in the comparison consisted of total net radiative flux (short-wave + long-wave balance) and global downward short-wave flux. The upward long-wave radiation flux was calculated using a downfacing IR thermometer giving surface temperature over full-grown crops. The downward long-wave radiation flux was calculated as a residual. The measured sunshine hours and total cloudiness from the SYNOP observations were used as additional information.

The predicted and observed downward short-wave and long-wave radiation fluxes together with the predicted integrated cloud condensate content and predicted and observed total cloud cover are shown in Figure 5. The calculated values differ from the observed ones most in those cases (e.g. 12 UTC 15 July) where the observed and predicted total cloud cover differ most, and where the predicted cloud condensate contents probably also differ from the true values. The 'H2 old' and 'H2 new' results are close. The new parametrization gives slightly greater SW and LW fluxes at the surface in cases in which an upper ice cloud was predicted by the model (e.g. 16 and 17 July 12 UTC). In the case of thick mixed and water clouds with moderate cloud condensate amount (e.g. 11 and 12 July, 12 UTC) the diagnosed $r_{e,\mathrm{SW}}$ values in the low troposphere are quite small, and consequently the SW flux through the clouds is slightly smaller in 'H2 new'. In the other cases the fluxes given by the new scheme are approximately equal to those of the old scheme.

5.5 Influence of radiation parametrizations on a forecast

The influence of the proposed parametrization on a forecast is illustrated by a study of the convective case of 9 July 1996. Two HIRLAM experiments with a horizontal resolution of 27 km, 31 levels in the vertical and a 2-min time step are compared. In both experiments a mass-flux type convection parametrization is used (Tiedke, 1989). The forecasts are initialised with the 00 UTC analysis.

A frontal system connected with a low pressure centre over the Southern Baltic Sea was moving northwards over Scandinavia. Heavy rainfall and a record high amount of lightning were registered in Southern Finland. The surface temperature difference between the warm and cold air masses was of the order of 20 K. The surface pressure and integrated cloud condensate amount at 12 UTC as predicted by the reference HIRLAM model with the old radiation parametrization are shown in Figure 6.

The overall synoptic features of the forecast are almost unchanged by the proposed parametrization changes. The mean net radiation flux (short-wave + long-wave) over all 13 000 grid points of the whole integration area at the surface of the +12 hour forecast using the 'H2 new' scheme is 27 W m^{-2} greater than that given by 'H2 old'.

Changing the radiation parametrization of clouds changes the two-metre temperature. This gives a tool to study the impact of the modifications to the radiation scheme. The average two-metre temperatures are practically equal in the two experiments. The maximum local differences of T_{2m} given by the new and the old schemes in the +12 hour forecast (Figure 7) are -3...+5 K. The difference is mainly

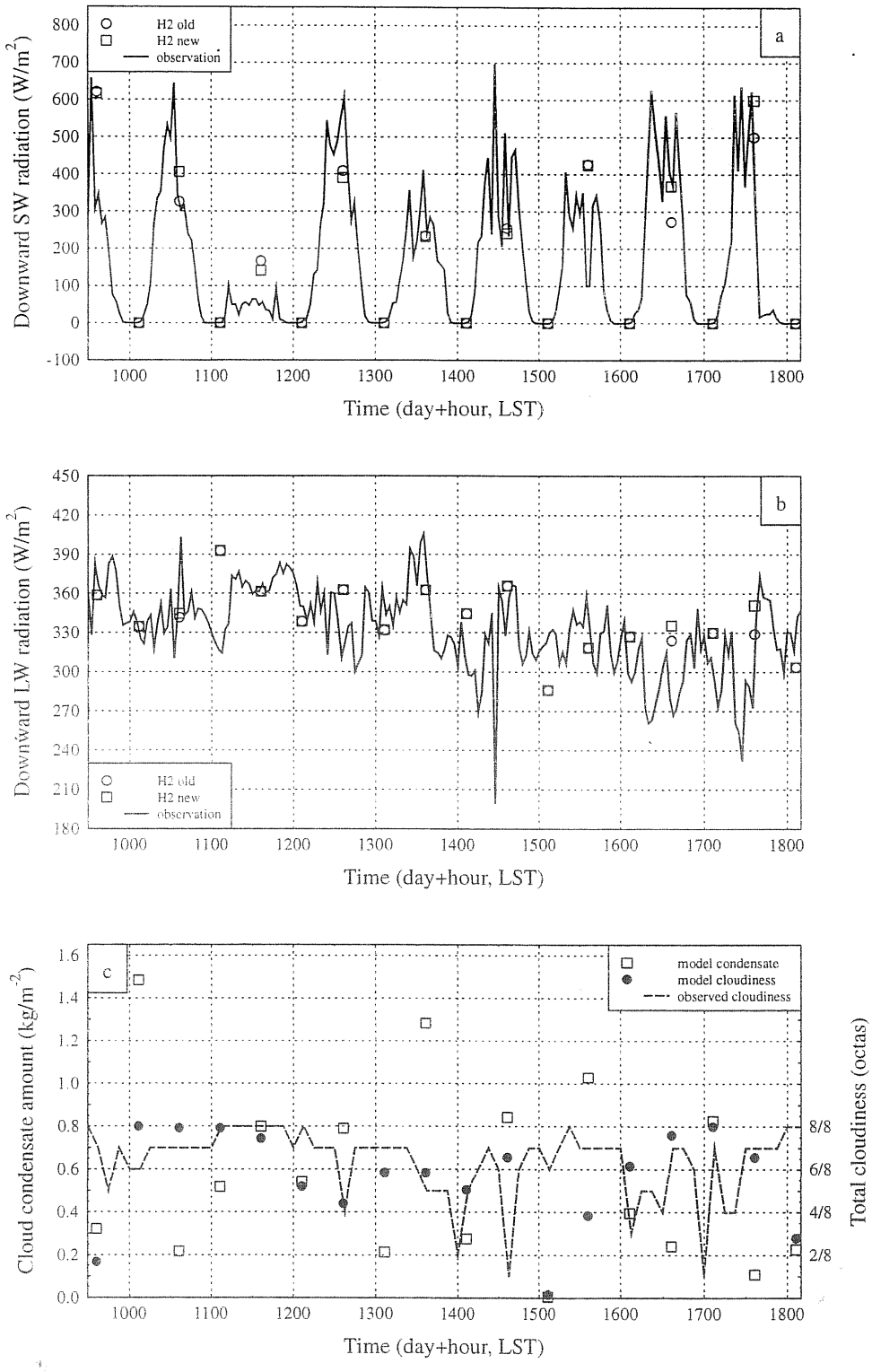

Figure 5: Downward short-wave (a) and long-wave (b) radiation fluxes at Jokioinen from 12 UTC 9 July to 12 UTC 19 July, 1989. Observed fluxes are shown with a solid line, 'H2 new' results with squares and 'H2 old' results with circles. Predicted integrated cloud condensate amount (squares), predicted (dots) and observed cloudiness (dashed line) are shown in (c). Time shown as days in July, 1989, local solar time used.

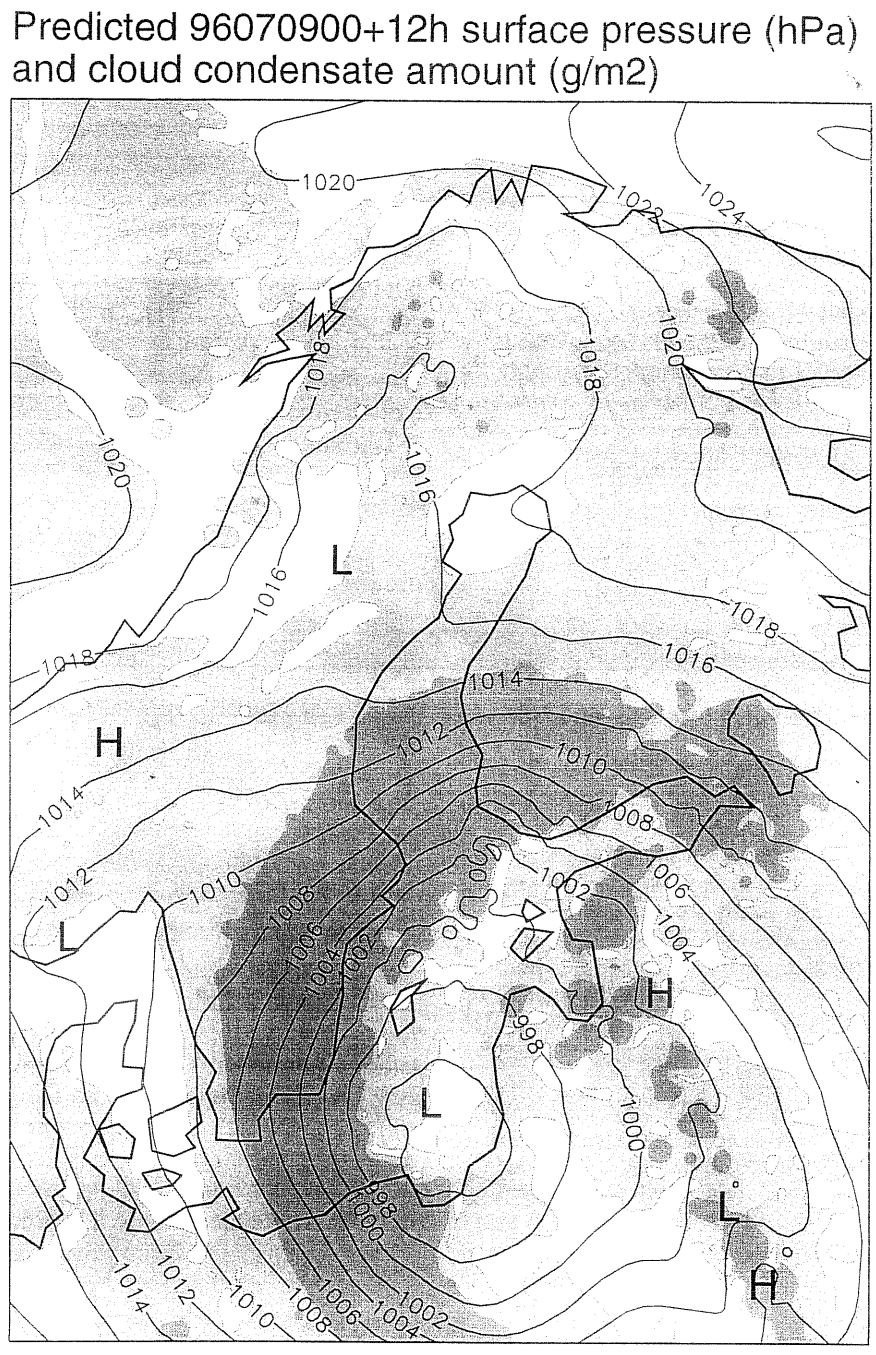

Figure 6: The reference HIRLAM forecast at 00 UTC 9 July 1996 +12h. Isolines: surface pressure at an interval of 2 hPa. Over the shaded light grey areas the integrated cloud condensate amount is greater than 50 gm^{-2}, over the dark grey areas greater than 250 gm^{-2}.

seen over areas with thin clouds, since the thickest clouds are opaque in either scheme. Over the areas of maximum differences, the 'H2 new' scheme seems to give temperatures somewhat closer to observed than the 'H2 old' scheme. In the +24 hour forecast valid at night the temperature difference between the schemes is insignificant.

Horizontal and vertical distribution of cloudiness differ somewhat in the experiments. However, the ver-

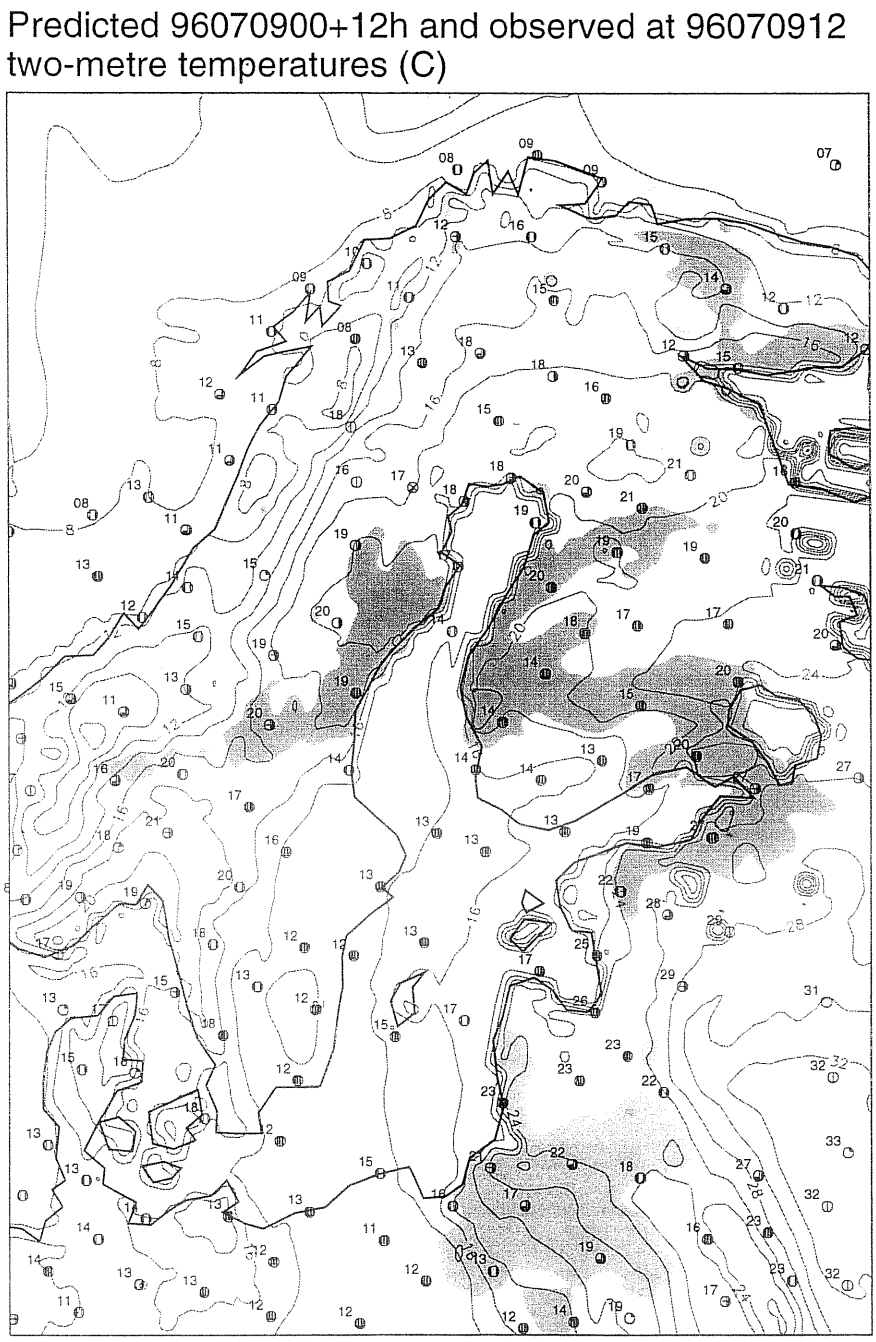

Figure 7: Two-metre temperature and cloud cover observed at 12 UTC 9 July, 1996 (values plotted at synoptic stations) and predicted by the 'H2 new' experiment, based on the analysis at 00 UTC 9 July (solid curves with an interval of 2 K). Difference between the predicted using the new and the old radiation parametrization two-metre temperature $T_{2m,new}$ - $T_{2m,old}$: over the light grey areas the difference is smaller than −2 K, over the dark grey areas it is greater than +2 K.

tically integrated cloud condensate path, averaged over the whole integration area, does not change significantly. The suggested changes in the radiation parametrization influence the cloud-radiation interactions in a complex way. Direct radiative heating and cooling may influence condensation and evaporation in clouds. Differences in cloudiness change the surface energy balance which in turn may lead

to changes in convective processes. These changes might have an impact to other physical and dynamical processes of the model. In the case studied such an impact could not be surely identified.

6 Conclusions

The effective radius r_e is retrieved from the cloud condensate content for water clouds and from the temperature for ice clouds. The HIRLAM radiation scheme is extended to be able to handle clouds with different sizes of cloud droplets and ice crystals in a realistic way. The fast performance of the model is not affected, because r_e is used in the framework of the existing scheme. Tuning of the empirical parameters of the scheme has a clear physical basis.

The effect of the new parametrization is best seen in the short-wave fluxes. In the ICRCCM comparisons, the difference between small-drop and large-drop clouds is significant and well reproduced by the new scheme. Introduction of the effective radius makes the scheme more sensitive to the vertical distribution of cloud water and ice. High clouds consisting of ice crystals with large effective radii are less reflective than the high water clouds of the old scheme. The long-wave fluxes given by the proposed scheme differ from those of the present scheme only in the case of thin clouds.

In the JASIN case, the new scheme, when used to calculate radiation fluxes through a thick stratus cloud, gives results near to those observed. Comparison of calculated and observed surface radiation fluxes at Jokioinen shows that the new parametrization gives slightly greater surface SW and LW fluxes in the presence of upper ice cloud. In the case of thick but not too dense mixed and water clouds the SW flux through the clouds is slightly smaller in the new than in the old parametrization. The predicted two-metre temperatures given by full three-dimensional HIRLAM experiments, using the new and the old radiation parametrizations, are close to each other on average. However, maximum local daytime differences between the experiments were found in the range -3...+5 K.

Comparison of model radiation fluxes with those observed by routine surface measurements, by field studies (including in-cloud observations), and by satellites is needed in the validation and future development of the scheme. More synoptic cases are to be studied with the full three-dimensional model to compare the impact of the modifications with observations.

References

Baer F., Arsky N., Charney J.J., and Ellingson R.G., 1996: Intercomparison of heating rates generated by global climate model longwave radiation codes. J. Geophys. Res. **101**, 26589–26603.

Bower K.N., Choularton T.W., Latham J., Nelson J., and Baker M.B., 1994: A parameterization of warm clouds for use in general circulation models. J. Atmos. Sci. **51**, 2722–2732.

Chen C.-T. and Ramaswamy V., 1996: Sensitivity of simulated global climate to perturbations in low-cloud microphysical properties. Part I: Globally uniform perturbations. J. Climate **9**, 1385–1402.

Chou M.-D., 1986: Atmospheric solar heating in the water vapour bands. J. Appl. Meteor. **25**, 1532–1542.

Chylek P., Damiano P., Ngo D., and Pinnick R., 1992: Polynomial approximation of the optical properties of water clouds in the 8–12 μm spectral region. J. Appl. Meteor. **31**, 1210–1218.

Dandin P., Pontikis C., and Hicks E., 1997: Sensitivity of a GCM to changes in the droplet effective radius parameterization. Geoph. Res. Letters, **24**, 437–440.

Ebert E.E. and Curry J.A., 1992: A parameterization of ice cloud optical properties for climate models. J. Geophys. Res. **97**, 3831–3836.

Ellingson R.G., Ellis J., and Fels S., 1991: The intercomparison of radiation used in climate models: Longwave results. J. Geophys. Res. **96**, 8929–8954.

Ellingson R.G. and Fouquart Y., 1991: The intercomparison of radiation used in climate models: An overview. J. Geophys. Res. **96**, 8925–8927.

Fu Q., 1996: An accurate parameterization of the solar radiative properties of cirrus clouds for climate models. J. Climate **9**, 2058–2082.

Gultepe I. and Isaac G.A., 1996: The relationship between cloud droplet and aerosol number concentrations for climate models. Int. J. Climatol. **16**, 941–946.

Gultepe I., Isaac G.A., Leaitch W.R., and Banic C.M., 1996: Parameterizations of marine stratus microphysics based on in situ observations: Implications for GCMs. J. Climate **9**, 345–357.

Han Q., Rossow W.B., and Lacis A.A., 1994: Near-global survey of effective radii in liquid water clouds using ISCCP data. J. Climate **7**, 465–497.

Heymsfield A.J. and Platt C.M.R., 1984: A parameterization of the particle size spectrum of ice clouds in terms of the ambient temperature and ice water content. J. Atmos. Sci. **41**, 846–855.

Hu Y.X. and Stamnes K., 1993: An accurate parameterization of the radiative properties of water clouds suitable for use in climate models. J. Climate, **6**, 728–742.

Källen E., 1996: HIRLAM documentation manual, system 2.5. Available from SMHI, S-60176 Norrköping.

Kiehl J.T., 1994: Sensitivity of a GCM climate simulation to differences in continental versus maritime cloud drop size. J. Geophys. Res. **99**, 23107–23116.

Liou K.N. and Wittman G.D., 1979: Parameterization of the radiative properties of clouds. J. Atmos. Sci. **36**, 1261–1273.

Martin G.M., Johnson D.W., and Spice A., 1994: The measurement and parameterization of effective radius of droplets in warm stratocumulus clouds. J. Atmos. Sci. **51**, 1823–1842.

Matvejev L.T., 1984: Cloud dynamics. D. Reidel Publishing Company, 340pp.

Ou S.-C. and Liou K.N., 1995: Ice microphysics and climatic temperature feedback. Atmos. Res. **35**, 127–138.

Pontikis C., 1996: Parameterization of the droplet effective radius of warm layer clouds. Geophys. Res. Lett. **23**, 2629–2632.

Ramaswamy V. and Freidenreich S.M., 1992: A study of broadband parametrizations of the solar radiative interactions with water vapor and water drops. J. Geophys. Res. **97**, 11487–11512.

Roeckner E., Arpe K., Bengtsson L., Christoph M., Claussen M., Dümenil L., Esch M., Giorgetta M., Schlese U., and Schulzweida U., 1996: The atmospheric general circulation model ECHAM-4: Model description and simulation of present-day climate. Report No. 218, Max-Planck-Institut für Meteorologie, Hamburg.

Sass B.H., Rontu L., and Räisänen P., 1994: HIRLAM-2 Radiation Scheme: Documentation and Tests. The HIRLAM 3 Project, c/o SMHI, S-60176 Norrköping, Technical Report No. 16.

Savijärvi H., 1990: Fast radiation parameterization schemes for mesoscale and short-range forecast models. J. Appl. Meteor. **29**, 437–447.

Savijärvi H., 1997: Short-wave optical properties of rain. Tellus **49**, 177–181.

Savijärvi H., Arola A., and Räisänen P., 1997: Shortwave optical properties of precipitating waterclouds. Q. J. R. Meteorol. Soc. **123**, 883–899.

Schmetz J., 1987: Measured and calculated solar fluxes through a stratocumulus cloud observed during the JASIN experiment. An unpublished note included in the material sent to ICRCCM participants on November 16, 1987.

Schmetz J., Raschke E., and Fimpel F., 1981: Solar and thermal radiation in maritime stratocumulus clouds. Contr. Atmos. Phys. **54**, 442–452.

Slingo A., 1989: A GCM parameterization for the shortwave radiative properties of water clouds. J. Atmos. Sci. **46**, 1419–1427.

Slingo A., 1990: Sensitivity of the Earth's radiation budget to changes in low clouds. Nature, **343**, 49–51.

Slingo A., Nicholls S., and Schmetz J.,, 1982: Aircraft observations of marine stratocumulus during JASIN. Q. J. R. Meteorol. Soc. **108**, 833–856.

Slingo A. and Schrecker H.M., 1982: On the shortwave radiative properties of stratiform water clouds. Q. J. R. Meteorol. Soc. **108**, 407–426.

Stephens G.L., 1978: Radiation profiles in extended water clouds. I: Theory. J. Atmos. Sci. **35**, 2111–2122.

Sundqvist H., 1993: Inclusion of ice phase of hydrometeors in cloud parameterization for mesoscale and largescale models. Contr. Atmos. Phys. **66**, 137–147.

Sundqvist H., Berge E., and Kristiánsson J.E., 1989: Condensation and cloud parameterization studies with a mesoscale numerical weather prediction model. Mon. Wea. Rev. **117**, 1641–1657.

Tiedtke M., 1989: A comprehensive mass flux scheme for cumulus parameterization in large scale models. Mon. Wea. Rev. **117**, 1779–1800.

Westphal D.L., Kinne S., Pilewskie P., Alvarez J.M., Minnis P., Young D.F., Benjamin S.G., Eberhard W.L., Kropfli R.A., Matrosov S.Y., Snider J.B., Uttal T.A., Heymsfield A.J., Mace G.G., S H.M., Starr D.O., and Soden J.J., 1996: Initialization and validation of a simulation of cirrus using FIRE-II data. J. Atmos. Sci.**53**, 3397–3429.

Wyser K., 1998a: The effective radius in ice clouds. J. Climate, **11**, 1793–1802.

Wyser K., 1998b: The effective radius in large-scale models: impact of aerosols and coalescence. Atmos. Res. **49**, 213–234.